CHEMISTRY
A EUROPEAN JOURNAL

DOI: 10.1002/chem.201002190

SBA-15-Type Organosilica with 4-Mercapto-*N*,*N*-bis-(3-*Si*-propyl)butanamide for Palladium Scavenging and Cross-Coupling Catalysis

Samir El Hankari,[a, b] Abdelkrim El Kadib,[c] Annie Finiels,[a] Ahmed Bouhaouss,[b] Joël J. E. Moreau,[a] Cathleen M. Crudden,[c] Daniel Brunel,[a, d] and Peter Hesemann*[a]

Abstract: This work describes the synthesis of novel functional silica materials with difunctional thiol–amide substructures and featuring regular architectures on a mesoscopic level. The functional materials were synthesised by both one-pot co-condensation and post-grafting approaches. The thiol groups confined in the matrix were found to be efficient for palladium entrapment, leading to highly active and reusable heterogeneous catalysts for Sonogashira and Suzuki–Miyaura cross-coupling reactions. This work evidences the crucial role of both the thiol precursor and the condensation degree of the silica scaffold in view of the design of stable and reusable tailor-made mesoporous catalytic silica materials.

Keywords: cross-coupling · heterogeneous catalysis · mesoporous materials · palladium · template synthesis

Introduction

Since their first preparation in the early 1990s,[1] nanostructured silica-based materials obtained by templating routes[2] have gained considerable interest due to their good thermal stability, high porosity and narrow pore-size distribution. These features make mesoporous silica-based materials ideal candidates for applications in various fields such as catalysis,[3] separation[4] and detection.[5]

For most applications, the introduction of functional groups on the surface of the material is critical for chemoselectivity. Among such functionalised materials, mercaptopropyl-functionalised nanostructured silica materials have been studied since the late 1990s. Functionalisation with thiol groups can be achieved either by post-grafting[6,7] or one-pot hydrolysis–polycondensation procedures.[8–11] The resulting sulphur-containing materials show interesting features for metal adsorption and therefore have found widespread applications in separation, in particular for the sequestration of heavy metals such as mercury, palladium or platinum.[7,9,12] The kinetics of mercury uptake on various types of thiol-functionalised mesoporous silica have been examined to reveal the morphologies of the materials on a mesoscopic length scale and to provide detailed information concerning the distribution of thiol groups throughout the material.[13] In particular, it has been shown that the synthetic pathway (post-grafting or co-condensation) has a strong influence on the binding properties of the immobilised thiol groups in terms of the degree of accessible thiol sites, adsorption kinetics and stability of the resulting material.[14] Besides nanostructured silicas, bifunctional thiol-containing periodic mesoporous organosilicas (PMO) have also been considered in solid–liquid extraction of heavy metals. More hydrophobic PMO-type materials obtained from silylated organic precursors containing *p*-phenylene[15] or isocyanurate[16] groups on the one side and mercaptopropyl-trialkoxysilane on the other side show similar features in metal sequestration compared with thiol-functionalised mesoporous silica[17] and effectively remove "soft" metal ions such as Hg^{2+} and Ag^{+} from aqueous solutions, whereas lower affinities were observed for the "harder" metal ions Cd^{2+}, Co^{2+} and Pb^{2+}.

Mesoporous silicas containing thiol groups are also interesting intermediates to access materials with anionic sulfonic

---

[a] S. El Hankari, Dr. A. Finiels, Prof. J. J. E. Moreau, Dr. D. Brunel, Dr. P. Hesemann
Institut Charles Gerhardt de Montpellier
Équipes AM2N and MACS
Ecole Nationale Supérieure de Chimie de Montpellier
8, rue de l'Ecole Normale
34296 Montpellier Cedex 05 (France)
Fax: (+33) 467-1443-53
E-mail: peter.hesemann@enscm.fr

[b] S. El Hankari, Prof. A. Bouhaouss
Laboratoire de Chimie Physique Générale I des Matériaux
Nanomatériaux et Environnement
Université Mohammed V - Agdal
Faculté des Sciences
Av. Ibn Battouta, Rabat (Maroc)

[c] Dr. A. El Kadib, Prof. C. M. Crudden
Department of Chemistry
Queen's University
90 Bader Lane
K7L 3N6 Kingston, Ontario (Canada)

[d] Dr. D. Brunel
Instituto de Tecnologia Quimica
UPV-CSIC–Universidad Politecnica de Valencia
Av. de los Naranjos s/n
46022 Valencia (Spain)

Supporting information for this article is available on the WWW under http://dx.doi.org/10.1002/chem.201002190.

acid groups, which can easily be prepared by oxidation reactions. These materials can be used as ion-exchange resins,[11] solid acid catalysts[18] or hard templates for the formation of tube-like carbon replicas.[10]

More recently, Crudden and others showed that thiol containing mesoporous silicas are excellent scavengers and heterogeneous ligands for palladium-based catalysts.[14,19,20] High catalytic activity and recyclability were observed in Pd-catalyzed cross-coupling reactions such as the Suzuki–Miyaura and Mizoroki–Heck reactions. In these materials, a beneficial effect on the catalytic properties was attributed to the SBA-15-type mesostructure, restricting the growth of palladium nanoparticles based on the size of the channels. Whereas Pd adsorbed on amorphous silica agglomerated into large particles on the exterior of the surface, leading to catalytic deactivation, palladium particles that formed on the SBA-15-based support were limited by the size of the channels to approximately 6 nm.[14] Although the materials could be reused multiple times, eventually degradation due to collapse of the walls took place, which was shown to be caused by the necessary presence of a strong base for these coupling reactions.[21] The incorporation of aluminium was shown to dramatically improve stability, but since Pd appears to reside primarily on the interior of these structures, a pore wall collapse leads to loss of catalytic activity as it entraps Pd inside.[21] Interestingly, this was not the case with the more open cubic KIT-6-type supports, which remain catalytically active after 6–8 runs, despite the collapse of the mesostructure.[22] The presence of Pd on the exterior of these materials was confirmed by TEM studies, and, consistent with the lack of mesoporosity at this point, Pd was agglomerated into large, non-uniform particles. Thus the design of materials that are able to retain Pd on the interior surface in the same way that SBA-15-type structures are able to do, but that are stable towards base-induced pore collapse is a significant and important challenge in this area.

Detailed studies on this system gave a deep insight in the reaction mechanism and showed that the reaction likely occurs in homogeneous solution following a “release and catch” mechanism.[14,23] Catalytic Pd-species are leached out of the materials, then they carry out the coupling reaction, and redeposit at the end of the catalytic cycle. Thiol-functionalised mesoporous silicas are particularly efficient for the recapture of metallic species at the end of the catalytic cycle and thus ensure low Pd contamination of the reaction mixture and products. This feature is of great interest for the regulatory issue of metal contamination in the context of pharmaceutical synthesis. Many bioactive substrates are prepared by Pd-based catalysts that necessitate a time consuming work-up and costly effective techniques for metal removal.[24,25] The preparation of highly conjugated materials for use in organic electronics has even more stringent requirements for metal contamination since the presence of small quantities of metal can act as locations for short circuits.

In view of designing more sophisticated catalysts for palladium cross-coupling reactions, several parameters have to be considered: 1) the topology and the structure type of the support influences the mass transfer and diffusion of metallic species;[22,26] 2) the pore size of the material has to be high enough to ensure diffusion of reactants and products to and from the active site; it should avoid any mass-transport limitation;[27] 3) the homogeneous distribution of the active sites over the whole material (for instance, wall framework vs. pores) should facilitate the accessibility of the reactants to the active site and, 4) the hydrophilic–hydrophobic balance and the surface states of the support should permit the host–guest interactions and adsorption–desorption process of the reactants and products.[28] Based on these criteria, we began to investigate new nanostructured materials based on sulphur-containing SBA-15-type structures. The use of a new bis-silylated amido–thiol as a polymerisable precursor allowed us to synthesise novel wall- and pore-functionalised siliceous materials. Because the nature of the precursors employed has a pivotal role in the templating process,[29,30] we were especially interested to study the repercussions of the use of a disilylated precursor on the morphology of the resulting materials and, consequently, on the accessibility of the thiol groups and the resulting catalytic activity of these materials. Compared with previous work employing monodentate grafting sites, the new materials should have greater stability of the thiolated surface under aqueous conditions, and should also have different surface chemistry based on the inclusion of a polar amide in the linker. For the sake of comparison, grafted material was prepared starting from a pure inorganic SBA-15 material, and comparisons made to previously reported MPTMS-functionalised materials. The accessibility of thiol groups was assessed by scavenging palladium in THF solution. The resulting palladium-supported materials were used as catalysts for Sonogashira and Suzuki–Miyaura cross-coupling reactions and comparisons made to more conventional MPTMS-functionalised materials.

Results and Discussion

Although recent studies have examined the effect of parameters such as the method of incorporation of the thiol, the architecture of the material, and the pore size of the thiol-functionalised material on catalytic properties and stability,[20–22,31] the influence of the structure of the thiol precursor on the morphology of the formed mesoporous silica and the catalytic performances of the obtained Pd-impregnated nanostructured materials has not been examined to date. Thus, we targeted an original precursor with two points of attachment through an amide linker, aiming to uniformly functionalise the silica wall framework. This compound was used to synthesise amide–thiol-functionalised mesoporous silica, both through post-grafting and co-condensation approaches. The catalytic properties of the resulting Pd-impregnated materials were compared to classical mercaptopropyl-functionalised silica obtained from mercaptopropyltriethoxysilane (MPTES) by direct hydrolysis–co-condensation with tetraethoxysilane (TEOS) and subsequent Pd-impregnation.

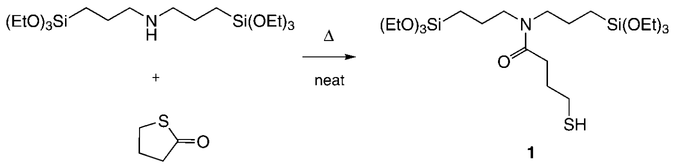

Scheme 1. Synthesis of the disilylated thiol–amide precursor **1**.

Precursor and materials synthesis and characterisation: The preparation of the disilylated 4-mercapto-*N*,*N*-bis(3-(triethoxysilyl)propyl)butanamide precursor **1** was derived from a previous preparation of 4-mercapto-*N*-(3-(triethoxysilyl) propyl)butanamide, obtained by the ring opening of γ-thiobutyrolactone with monosilylated 3-aminopropyltriethoxysilane.[32] A similar ring opening of γ-thiobutyrolactone by nucleophilic attack of bis(triethoxysilylpropyl)amine afforded the targeted product **1** after elimination of volatile products and starting materials (Scheme 1). This new bis-silylated compound was characterised by ^{1}H, ^{13}C, infra-red and mass spectroscopic analysis. The ^{13}C attached proton test (APT) liquid NMR spectrum of the precursor **1** is shown in Figure 1. The presence of the amide group with its partial double-bond character results in a doubling of the ^{13}C and the ^{1}H liquid NMR spectra. 2D NMR spectroscopy (see the Supporting Information) permitted an accurate attribution of the carbon centres present in the precursor.

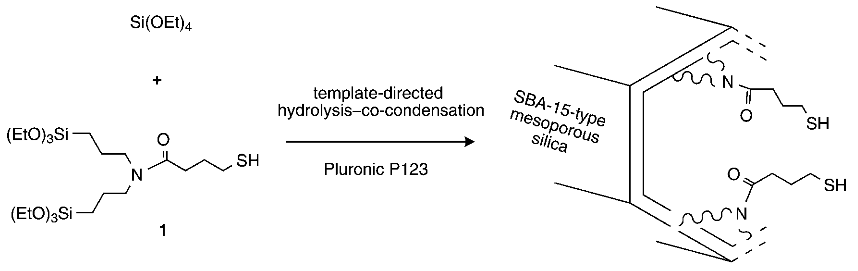

Scheme 2. Template-directed hydrolysis/polycondensation of precursor **1** with tetraethyl-*ortho*-silicate.

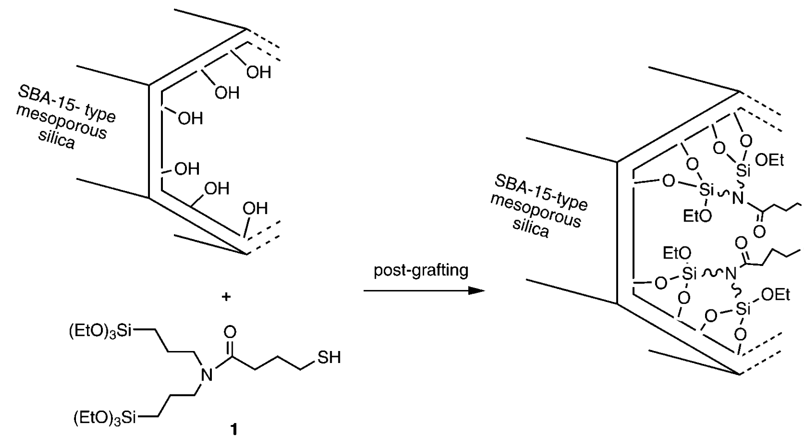

Scheme 3. Synthesis of material SBA-15-G by post-synthesis grafting of precursor **1** onto the SBA-15-type silica.

Thiol–amide-functionalised materials were obtained either by using template-directed hydrolysis/polycondensation of precursor **1** with various amounts of a silica network precursor (tetraethyl-*ortho*-silicate, TEOS, Scheme 2) or post-grafting reactions of precursor **1** onto a previously synthesised SBA-15-type silica (Scheme 3). Whereas post-synthesis grafting reactions afforded materials in which the whole silylated precursor is grafted onto the surface of the mesoporous silica, one-pot hydrolysis polycondensation reactions led to the formation of materials in which the siloxy groups of the thiol precursor are integrated in the silica network and therefore are an inherent part of the silica scaffold.

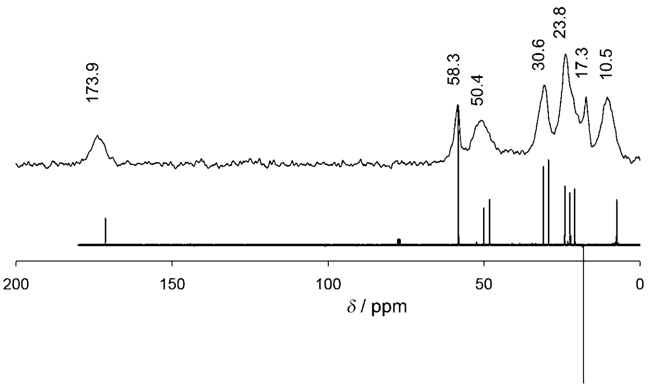

Figure 1. ^{13}C APT liquid NMR spectrum of precursor **1** (bottom) and ^{13}C CP MAS NMR spectrum of material SBA-15-G (top).

In the first series of experiments, the bis-silylated precursor **1** was employed for the synthesis of functional silica-hybrid materials by using a co-condensation approach. Hydrolysis–polycondensation reactions were performed with thioamide **1**:TEOS ratios of 1/2, 1/4, 1/6 and 1/8, to give the formation of the materials SBA-15-(1/2), SBA-15-(1/4), SBA-15-(1/6) and SBA-15-(1/8), respectively. Another material (SBA-15-(1/8-KCl)) was synthesised in the presence of potassium chloride to evaluate the influence of the presence of mineral salts on the formation of nanostructured materials in hydrolysis–polycondensation reactions. All the above materials were synthesised in the presence of the non-ionic triblock-copolymer Pluronic P123 as the structure-directing agent following previously published procedures for co-condensation reactions of di- and oligosilylated precursors with TEOS.[30,33] The exact quantities and ratios of precursor **1** and TEOS in the various formulations are given in Table 1.

Table 1. Molar precursor **1**/TEOS ratios and loadings of the amide–thiol-functionalised materials.

Material	Precursor **1** [mg (mmol)]	TEOS [mg (mmol)]	Surfactant P123 [mg]	HCl_{aq} (1.9 M) [mL]	Loading[a] SiO_2 [mmol g^{-1}]
SBA-15-(1/2)	121 (0.23)	97 (0.46)	91	2.8	2.75
SBA-15-(1/4)	540 (1.03)	850 (4.1)	500	16	2.75
SBA-15-(1/6)	390 (0.73)	915 (4.39)	500	16	2.23
SBA-15-(1/8)	300 (0.58)	950 (4.55)	500	16	1.77
SBA-15-(1/8-KCl) [b]	300 (0.58)	950 (4.55)	500	16	2.20 (1.99)[c]
SBA-15-G	–	–	–	–	1.48 (1.33)[c]

[a] Values obtained by TGA measurements. [b] KCl amount: 3.17 g (42.5 mmol). [c] Values obtained by ^{29}Si OP-MAS NMR measurements.

A functionalised material was also synthesised by a post-grafting reaction. In this synthesis, the bis-silylated precursor was anchored on the surface of previously synthesised SBA-15-type silica, giving rise to the material denoted SBA-15-G.

The obtained materials were characterised by means of solid state NMR spectroscopy and thermogravimetry to determine the loading of the materials. Nitrogen sorption experiments, X-ray diffraction and electron microscopy permitted us to gain detailed insight into the architecture of the thiol-functionalised materials.

The comparison of the materials obtained by post-synthesis grafting procedures and "one-pot" hydrolysis polycondensation procedures revealed different characteristics in terms of functionalisation degree and morphology.

Firstly, ^{13}C CP-MAS NMR spectroscopy provided a method for monitoring the incorporation of the amide–thiol substructures within the materials. The solid state ^{13}C cross-polarization magic angle spinning (CP-MAS)-NMR spectrum of material SBA-15-G is shown as an example in Figure 1. The spectrum clearly shows the characteristic signals of the aliphatic substructures ($\delta = 10$–50 ppm) and the signal of the carbonyl group at $\delta = 174$ ppm, which are both characteristic for the presence of the thiol–amide precursor within the materials. The signals at $\delta = 17$ and 58 ppm indicate the presence of uncondensed ethoxysilyl groups in the material. The solid state spectrum is in good agreement with the ^{13}C APT spectrum of precursor **1** (Figure 1, bottom) obtained in liquid NMR spectroscopy.

The ^{29}Si one pulse (OP)-MAS NMR spectra of materials SBA-15-(1/8-KCl) and SBA-15-G are shown in Figure 2. The ^{29}Si OP-MAS technique allows one to quantify the molar ratio of the different silicon species in the materials. Both spectra show the T- and Q-resonances characteristic of the presence of $RSiO_3$ and SiO_4 substructures. At first glance, the shape of the signals reflects the two different synthetic strategies applied for the synthesis of the two functional materials. In the case of the material SBA-15-(1/8)-KCl, a ratio of T and Q signals of 19.3/80.7 was found in the material. This ratio corresponds to a 0.96/8 ratio of the $RSiO_3$ and SiO_4 environments in the materials, which is in remarkable agreement to the molar ratio of the co-monomers in the reaction mixture (1/8). Besides the quantification of the T/Q-signal ratio, the spectra also gave further information concerning the degree of condensation the silicon centres in the materials. The spectra of SBA-15-(1/8-KCl) shows nearly equal amounts of Q^3 ($\delta = -101.2$ ppm) and Q^4 ($\delta = -110.2$ ppm) environments together with a very small amount of Q^2 species ($\delta = -91.1$ ppm). This result reflects the presence of a significant amount of Si–OH groups in the material. In contrast, the Q resonance in the spectrum of material SBA-15-G is dominated by the Q^4 resonance corresponding to completely condensed $Si(OSi)_4$ substructures, indicating a highly condensed silica network. This material was obtained by calcination at 550 °C to eliminate the non-ionic structure directing agent prior to the grafting reaction with precursor **1**. For this reason, the silica scaffold shows approximately 95 % condensation, which is a considerably higher value than that of the materials obtained under milder reaction conditions by "one-pot" hydrolysis–polycondensation procedures.

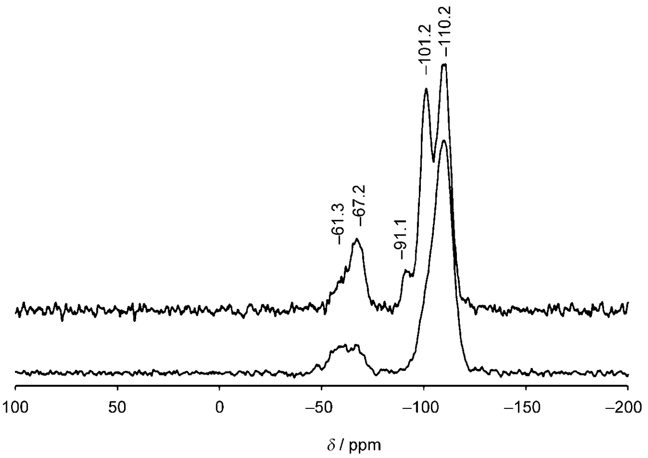

Figure 2. ^{29}Si OP MAS NMR spectrum of material SBA-15-(1/8-KCl) (top) and SBA-15-G (bottom).

The shape of the signals corresponding to the T resonances in Figure 2 reflects the degree of condensation of the $RSiO_3$ substructures. In the SBA-15-(1/8-KCl) material, a higher intensity was found for the T^3 substructure corresponding to fully condensed $RSi(OSi)_3$ sites. This result can be explained by the fact that the precursor **1** was completely incorporated within the silica walls during the hydrolysis–polycondensation reaction and reacted with hydrolyzed TEOS silica precursors. In contrast, the much broader shape of the T-resonances in the spectra of material SBA-15-G indicates the presence of nearly equal amounts of T^2 ($RSi(OSi)_2(OH)$) and T^3 ($RSi(OSi)_3$) sites. The quantification of the T^2/T^3 ratio in the materials using the dmfit program[34] shows that the molar ratio between the different T-species corresponds to $T^1/T^2/T^3 = 0.06{:}0.55{:}0.39$. Thus approximately 39 % of the siloxy groups of the amide–thiol precursor are anchored to the mesoporous silica walls through support by three Si−O−Si bonds. In addition, this explains the presence of residual ethoxy groups in the material that can be seen in the ^{13}C CP-MAS NMR spectrum of the material SBA-15-G.

The T/Q ratio found in the ^{29}Si OP-MAS NMR spectra of materials SBA-15-(1/8-KCl) and SBA-15-G directly gives the loadings of organic functionality in these solids. In the case of SBA-15-(1/8-KCl), a T/Q ratio of 0.193:0.807 was found, corresponding to a loading of 1.99 $mmol\,g^{-1}$ SiO_2. The material SBA-15-G has a slightly lower degree of functionalisation with a T/Q ratio of 0.138:0.862, corresponding to a loading of 1.33 $mmol\,g^{-1}$ SiO_2.

The characterisation of the materials by thermogravimetry gave additional quantitative information concerning the functionalisation degree of the materials. When the organic grafting was estimated from TGA measurements, the decomposed weight/residual (SiO_2) weight at 700 °C stems from organic grafted species on silica based on 1 g of silica. We used the following Equation (1) for the determination of the amount of immobilised organic entities. The results obtained are given in Table 1.

$$n_{\mathrm{thiol}} = \mathrm{org.\ wt\,\%}/[100-(\mathrm{org.\ wt\,\%}-\mathrm{H_2O\ wt\,\%})](\mathrm{M_{thiol}}-2\mathrm{H_2O}) \quad (1)$$

The results obtained from TGA measurements show that the TEOS/precursor ratio in the hydrolysis–polycondensation mixture has a direct influence on the loading of the resulting materials. The loadings of the materials are in the range of 2.75 $mmol\,g^{-1}$ SiO_2 for the material SBA-15-(1/2) and 1.77 $mmol\,g^{-1}$ SiO_2 in the case of the sample SBA-15-(1/8). Post-synthesis grafting led to a material with the lowest loading in this series (1.48 $mmol\,g^{-1}$ SiO_2). As expected, the use of higher amounts of the functional precursor in the hydrolysis–polycondensation mixtures yielded materials containing higher concentrations of immobilised organic substructures. The results of the TGA experiments are in good agreement with the results obtained from ^{29}Si OP-MAS NMR spectroscopy. The slightly higher loadings determined from TGA measurements can be explained by the presence of residual ethoxy groups in the materials as already concluded from ^{13}C CP-MAS NMR spectra of the solids. The degree of condensation of the T- and Q-silicon sites, as determined by ^{29}Si solid state NMR spectroscopy, clearly reflect the different synthetic pathways employed in the synthesis of the materials.

In the following, we addressed the determination of the morphologies of the obtained materials by means of X-ray diffraction, nitrogen sorption and electron microscopy. The textural properties of these materials are summarised in Table 2.

Table 2. Surface properties of the materials.

Material	XRD		Nitrogen sorption		
	d_{100} [Å]	a_o [Å]	BET surface area S_{BET} [$m^2 g^{-1}$]	Pore volume V_p [$mL\,g^{-1}$]	Average pore diameter D_p [Å][a]
SBA-15-(1/2)	–	–	260	–	–
SBA-15-(1/4)	–	–	442	0.64	86
SBA-15-(1/6)	92	106	583	0.68	74
SBA-15-(1/8)	80	104	608	0.71	72
SBA-15-(1/8-KCl)	103	119	568	0.93	89
SBA-15	98	113	614	1.02	89
SBA-15-G	99	114	314	0.48 (0.60)[b]	70

[a] Pore size evaluated according to the Broekhoff de Boer (BdB) method. [b] Pore volume versus pure silica weight.

Small-angle X-ray diffraction experiments gave the first information concerning the architectures of the materials. The diffractograms of the materials SBA-15-(1/2), SBA-15-(1/6), SBA-15-(1/8) and SBA-15-(1/8-KCl) are given in Figure 3. The results are summarised in Table 2. It is clear that the TEOS/precursor ratio in the hydrolysis–polycondensation mixture has a significant influence on the architecture of the materials synthesised by co-condensation reactions. Whereas the SBA-15-(1/2) materials do not show any diffraction pattern and are completely amorphous, increasing the ratio of TEOS in the hydrolysis–polycondensation mixtures led to materials with high structural regularity. The materials SBA-15-(1/6) and SBA-15-(1/8) display intermediate regularity. The diffractograms of these materials show intense (100) and weak (200) reflections, indicating that the materials have essentially worm-like or lamellar architectures. The addition of inorganic salts such as sodium chloride to the reaction mixture favours the formation of nanostructured materials with highly regular architectures.[35]

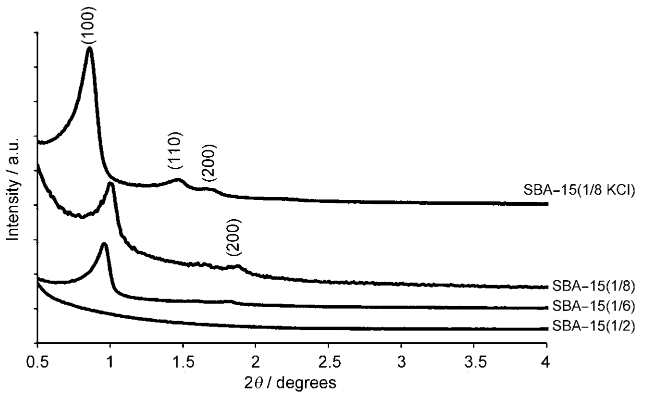

Figure 3. X-ray diffractograms of the materials SBA-15-(1/2), SBA-15-(1/6), SBA-15-(1/8) and SBA-15-(1/8-KCl), obtained by co-condensation of precursor 1 with TEOS

We have already employed this so-called “salt effect” to obtain nanostructured silica materials containing covalently tethered guanidinium sulfonimide ion pairs.[33] Consequently, the diffractogram of the material SBA-15-(1/8-KCl), synthesised in the presence of potassium chloride in the hydrolysis–polycondensation mixture, displays the 100, 110 and 200 reflections characteristic of nanostructured materials with hexagonal architectures on a mesoscopic length scale (Figure 3). It is noteworthy that the addition of potassium chloride to the hydrolysis–polycondensation mixture led to an increase of the pore–pore distance as can be seen from the shift of the (100) reflection from $2\theta = 0.96/0.99°$ ($a_0 =$ 106/104 Å) in the case of the materials SBA-15-(1/6) and SBA-15-(1/8) to $2\theta = 0.86$ ($a_0 = 119$ Å) observed for the material SBA-15-(1/8-KCl).

On the other hand, post-synthesis grafting reactions do not affect the architectures of nanostructured silica materials. The pristine SBA-15 silica and the material SBA-15-G show very similar diffractograms with nearly identical cell parameters (Table 2).

The results of the X-ray diffraction experiments were confirmed by nitrogen sorption experiments. The nitrogen sorption isotherms of the materials SBA-15-(1/2), SBA-15-(1/4), SBA-15-(1/6) and SBA-15-(1/8) are shown in Figure 4. The isotherms of the materials SBA-15-(1/8) and SBA-15-(1/8-KCl) are compared in Figure 5. Finally, the isotherms of the pristine silica SBA-15, used for post-grafting reactions, and the grafted material SBA-15-G are shown in Figure 7. The surface properties of these materials are summarised in Table 2.

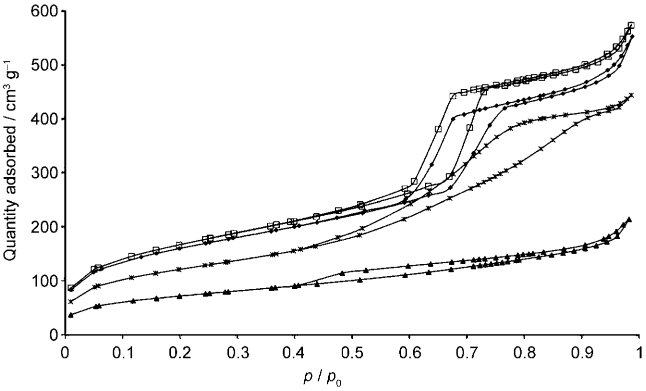

Figure 4. Nitrogen sorption isotherms of the materials SBA-15-(1/2) (▲), SBA-15-(1/4) (×), SBA-15-(1/6) (◆), SBA-15-(1/8) (□).

In the series of materials obtained by co-condensation reactions, materials SBA-15-(1/2) and SBA-15-(1/4) show nitrogen uptake over a large p/p_0 range, which indicates that these two materials display a low structural regularity and large pore-size distribution. Highly porous and structured materials were obtained starting from a **1**:TEOS ratio of 1/6. The material SBA-15-(1/6) has a specific surface area S_{BET} of $583\,\mathrm{m^2\,g^{-1}}$. The adsorption–desorption isotherm of this material shows a hysteresis loop in the range of $p/p_0 = 0.6$–0.7 indicating essentially mesoporosity with an average pore diameter of 86 Å. Slightly increased porosity and pore volume but very similar architecture on a mesoscopic length scale were found for the material SBA-15-(1/8).

The beneficial effect of mineral salts expected from previous reports[33,35,36] was evidenced in the case of material SBA-15-(1/8-KCl), which shows a very sharp adsorption step at $p/p_0 = 0.78$ indicating very narrow pore-size distribution centred at 89 Å. The nitrogen adsorption in the case of the material SBA-15-(1/8) occurs at lower pressures and is considerably flatter, which suggests a smaller average pore size and broader pore-size distribution in this material (Figure 5). Finally, the materials SBA-15-(1/8) and SBA-15-(1/8-KCl) show similar specific surface area as it can be seen from the very similar shape of the isotherms at low pressures ($p/p_0 < 0.4$; SBA-15-(1/8): $S_{\mathrm{BET}} = 608\,\mathrm{m^2\,g^{-1}}$; SBA-15-(1/8-KCl): $S_{\mathrm{BET}} = 568\,\mathrm{m^2\,g^{-1}}$) but considerably different pore volumes (SBA-15-(1/8): $0.71\,\mathrm{cm^3 g^{-1}}$ vs. SBA-15-(1/8-KCl): $0.93\,\mathrm{cm^3 g^{-1}}$).

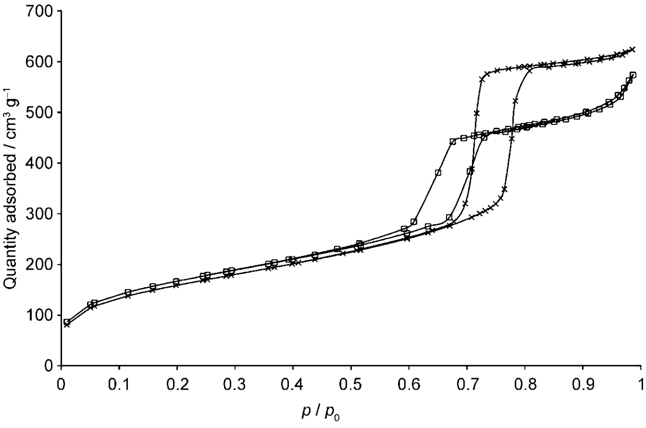

Figure 5. Nitrogen sorption isotherms of the materials SBA-15-(1/8) (□) and SBA-15-(1/8-KCl) (×).

This increase of the structural regularity in the case of the material SBA-15-(1/8-KCl), which is induced by the so-called “salt-effect”, can be rationalised by a swelling of the micelles together with a significant increase of the precursor/template interaction at the interface.[33,35,36] PEO-PPO-PEO triblock copolymers such as Pluronic P123 form micelles in water with poly(propyleneoxide) (PPO) cores surrounded by a shell of hydrated poly(ethylene oxide) (PEO) end blocks.[37] The presence of inorganic salts in the hydrolysis–polycondensation mixture induces dehydration of ethylene oxide layer, which decreases the hydrophilicity of PEO and enhances the hydrophobicity of PPO.[38] Thus, the less hydrophilic organosilicate precursor interacts in a favourable way with the template resulting in long-range-ordered domains of organosilica–surfactant–silica mesostructures.

From TGA measurements, it can be seen that the “salt-effect” increases the amount of organic molecules integrated in the wall of the materials. However, sufficient silica content is needed in order to “relax” the wall-framework of

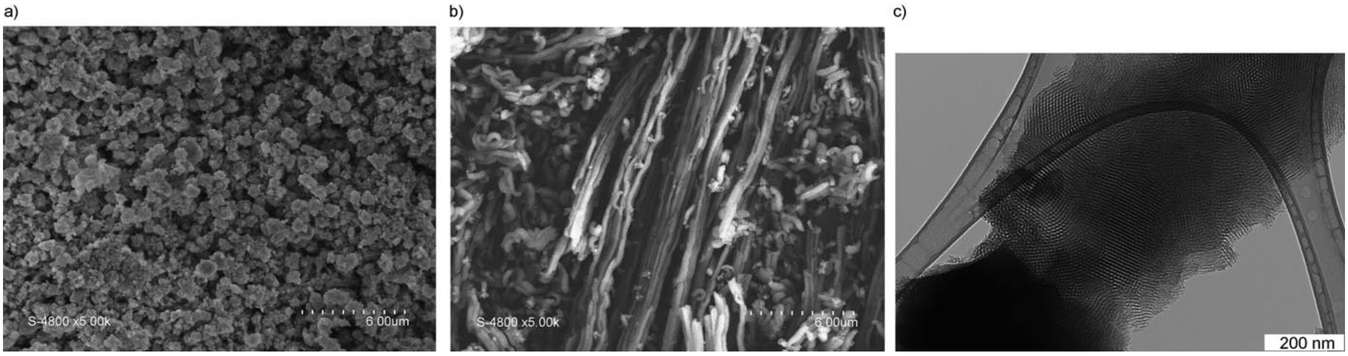

Figure 6. SEM pictures of materials a) SBA-15-(1/2) and b) SBA-15-(1/6); scale bar represents 6 μm. c) TEM image of material SBA-15-(1/8-KCl).

these hybrid materials. Consequently, materials with low silica content are amorphous or low-structured and show low porosity. In contrast, materials with high silica content display the typical features of SBA-type materials, that is, highly regular architectures on a mesoscopic length scale, mesoporosity and a very narrow pore-size distribution.

These results clearly indicate that the molar TEOS/**1** ratio in the hydrolysis–polycondensation mixture together with the presence of mineral salts are the most important parameters for the formation of nanostructured silica phases by co-condensation approaches for the synthesis of thiol functionalised materials from TEOS and the thiol-amide precursor **1**. The material SBA-15-(1/8-KCl) shows the highest structural regularity in this series.

Finally, the results obtained from nitrogen sorption and X-ray diffraction experiments were confirmed by transmission and scanning electron microscopy. An SEM image of material SBA-15-(1/2) given in Figure 6 shows the presence of agglomerated particles without any particular shape and diameters of approximately 1 μm. The particle shape observed in materials SBA-15-(1/6), SBA 1/8 and SBA-15-(1/8-KCl) is very different. Here, elongated particles and fibres (300–400 nm thick and up to 20 μm long) can be seen from the SEM images. The TEM image of material SBA-15-(1/8-KCl) (Figure 6c) reveals regular architectures on a mesoscopic length scale as already indicated from X-ray diffraction experiments.

The isotherms of materials SBA-15 and SBA-15-G, obtained through grafting of the precursor **1** on the surface of SBA-15, are shown in Figure 7. It is clear that the grafting reaction strongly affects the texture of the materials. The material SBA-15-G shows decreased values in terms of specific surface areas, pore volume and average pore diameter compared to the pristine silica SBA-15 (Table 2). The variation of the pore volume when standardised versus a pure silica weight of $1.02–0.6\ \mathrm{mL\,g^{-1}}$ SiO_2 results from the space occupied by the organic tether lining, and would correspond to a loading density of $1.67\ \mathrm{mmol\,g^{-1}}$ SiO_2 assuming the organic components are in a pseudo-liquid-phase state, which is in relatively good agreement with the value determined by TGA and ^{29}Si MAS NMR data. On the contrary, the architecture of these materials is not affected as indicated by the similar shape of the adsorption–desorption isotherms. This result is confirmed by the results of X-ray diffraction experiments with these two materials showing nearly identical cell parameters of the materials before and after grafting (Table 2).

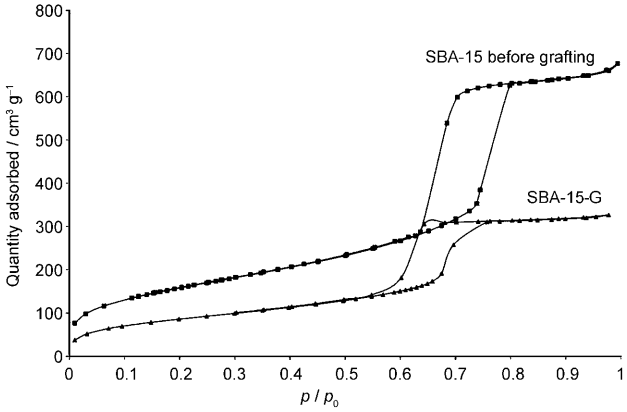

Figure 7. Nitrogen sorption isotherms of the materials SBA-15 and SBA-15-G.

Catalytic tests: To get a better understanding on the accessibility of thiol groups of the new reported materials SBA-15-(1/8-KCl) and SBA-15-G, we assessed their palladium scavenging ability. The materials were impregnated with palladium acetate in THF solution according to Scheme 4. Pd-uptake of the solid could easily be followed by immediate decolouration of the solution and the appearance of an orange colour on the mesoporous silica. Inductively coupled plasma (ICP)-MS analysis indicates that 99.92 and 99.97 % of palladium was removed from the solution to SBA-15-(1/8-KCl) and SBA-15-G, respectively. Initially, the quantity of palladium to be loaded was calculated based on the sulphur content of the material to give a S/Pd ratio of 2:1 since this ratio was shown to give the most active catalyst with the lowest leaching in catalytic studies.[14]

Having ascertained the capacity of thiolated groups to scavenge palladium, we directed our attention to study their catalytic behaviour in two important carbon–carbon bond-forming reactions: the Sonogashira[39,40] and Suzuki–

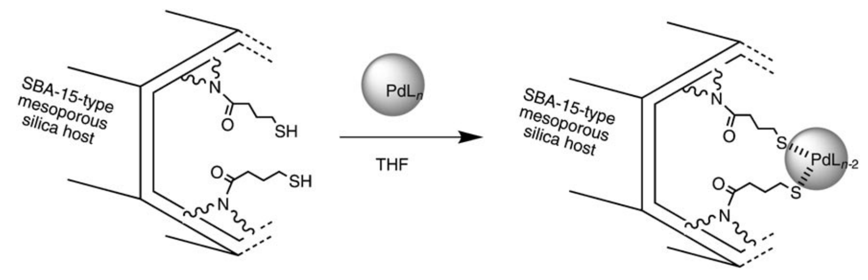

Scheme 4. Pd impregnation of the materials SBA-15-(1/8-KCl) and SBA-15-G.

Miyaura[41] cross-couplings. We began our study with the Suzuki–Miyaura reaction, which consists of coupling an aryl halide with an organoboron compound. To obtain a more accurate assessment of catalytic activity, electronically deactivated aryl bromides were chosen rather than the more easily coupled aryl iodides. We selected three coupling partners: 1-bromo-4-acetophenone **2**, 1-bromo-4-nitrobenzene **3** and 3-bromo-quinoline **4** (Scheme 5).

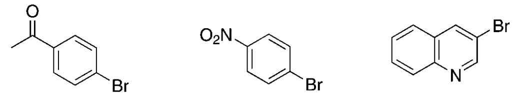

2 **3** **4**

Scheme 5. Aryl bromides **2–4** used as substrates in Suzuki–Miyaura and Sonogashira coupling reactions.

The results obtained with our catalysts SBA-15-(1/8-KCl)-Pd and SBA-15-G-Pd are systematically compared with the commonly used mercaptopropyl-mesoporous silica denoted as SBA-15-SH-Pd, obtained from mercaptopropyl-triethoxysilane (MPTES) by direct hydrolysis–co-condensation with tetraethoxysilane (TEOS) and subsequent Pd impregnation (Table 3). Under our conditions, no homo-coupling product was detected. Among the three coupling candidates, 1-bromo-4-nitrobenzene was the most reactive substrate because of its capacity to undergo a fast oxidative addition. Even though the three materials lead to quantitative cross-coupling, SBA-15-G-Pd and SBA-15-(1/8-KCl)-Pd are slightly more reactive compared with SBA-15-SH-Pd based on turn-over frequency (TOF), although a full kinetic assessment would need to be done to determine the exact magnitude of the differences.

Another cross-coupling reaction that has been less addressed in the context of thiolated materials is the Sonogashira reaction, despite the fact that this reaction is used extensively in the preparation of molecules for pharmaceutical and electronic applications. In this regard, we investigated the scope of our materials for the Sonogashira cross-coupling reaction (Table 4). Common protocols for the Sonogashira reaction involve the use of a copper source to assist the transmetallation of the alkyne.[39,42] We chose to employ copper-free conditions to avoid the possible contamination by a second metal. Much to our delight, the desired products were obtained selectively without side reactions and in high yield (up to 92 %, Table 4, entry 4). Similar to the Suzuki–Miyaura cross-coupling, 1-bromo-4-nitrobenzene **3** was found to be the most reactive substrate in this series resulting in complete consumption of the starting material in 40 min.

Table 3. Catalytic results in Suzuki–Miyaura-coupling reactions involving the haloarenes **2–4** and the Pd-containing materials SBA-15-(1/8-KCl)-Pd, SBA-15-G-Pd and SBA-15-SH-Pd.[a]

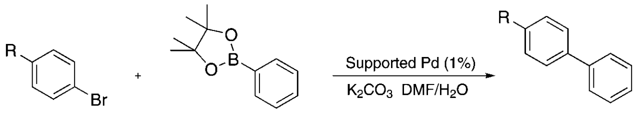

Entry	Substrate	Catalyst	t [h]	TOF [h^{-1}]	Yield [%][b]	Pd leaching [μg][c]	Pd leaching [%]
1	**2**	SBA-15-(1/8-KCl)-Pd	3.5	60	96	3.7	1.4
2	**2**	SBA-15-G-Pd	3	96	99	5.0	1.9
3	**2**	SBA-15-SH-Pd	7	88	96	0.66	0.25
4	**3**	SBA-15-(1/8-KCl)-Pd	3	84	94	2.4	0.9
5	**3**	SBA-15-G-Pd	3	116	98	4.2	1.6
6	**3**	SBA-15-SH-Pd	3	92	98	1.5	0.58
7	**4**	SBA-15-(1/8-KCl)-Pd	3	135	88	2.9	1.1
8	**4**	SBA-15-G-Pd	2.25	154	98	4.0	1.5
9	**4**	SBA-15-SH-Pd	4.5	92	93	1.9	0.7

[a] Arylbromide (1 equiv), phenylboronate (1.5 equiv). K_2CO_3 (2 equiv), Pd (1 mol %). [b] Calculated by GC using dimethoxybenzene as the internal standard. [c] Total Pd leached during the reaction.

An interesting feature of these thiolated materials resides in their high capacity to recapture leached palladium at the end of the reaction.[43] After recovering the materials by simple filtration, we were interested to assess the palladium contamination in the obtained biphenyl products. Palladium leaching was found to be low, despite the presence of functionality in the coupling partners. As expected, the Pd leaching was higher for the Sonogashira coupling compared with the products of the Suzuki–Miyaura cross-coupling. This can be attributed to the acetylene fragment, which is known to bind palladium and retain it in the product.[24] However, in all cases, the level of leaching is typically in the order of 1 % of the added catalyst in the Suzuki–Miyaura reaction and about 2–3 % of the added catalyst in the case of the more challenging Sonogashira reaction This corresponds to a total leaching of 5–10 μg of Pd.

Table 4. Catalytic results in Sonogashira-coupling reactions involving the haloarenes **2**–**4** and the Pd-containing materials SBA-15-(1/8-KCl)-Pd, SBA-15-G-Pd and SBA-15-SH-Pd.[a]

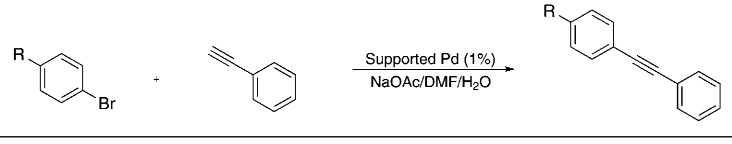

Entry	Substrate	Catalyst	*t* [h]	TOF [h^{-1}]	Yield [%][b]	Pd leaching [μg][c]	Pd leaching [%]
1	**2**	SBA-15-(1/8-KCl)-Pd	8	26	93	5.6	2.1
2	**2**	SBA-15-G-Pd	7.5	35	96	5.7	2.17
3	**2**	SBA-15-SH-Pd	8.5	16	92	7.4	2.8
4	**3**	SBA-15-(1/8-KCl)-Pd	0.66	92	92	7.2	2.7
5	**3**	SBA-15-G-Pd	0.66	348	96	6.5	2.45
6	**3**	SBA-15-SH-Pd	2	98	96	9.0	3.41
7	**4**	SBA-15-(1/8-KCl)-Pd	1	92	96	7.7	2.9
8	**4**	SBA-15-G-Pd	1.5	176	88	10.0	3.8
9	**4**	SBA-15-SH-Pd	3.5	106	88	8.3	3.14

[a] Arylbromide (1 equiv), phenylacetylene (1.5 equiv), NaOAc (2 equiv), Pd (1 mol %). [b] Calculated by GC using dimethoxybenzene as an internal standard. [c] Total Pd leached during the reaction.

For large scale applications, the high cost of palladium makes its recovery and reuse highly desirable. Hence, new heterogeneous candidates have to be assessed in terms of activity and selectivity, metal leaching resistance and catalyst lifetime and reusability considerations. With this aim, the recyclability of the three catalysts was investigated in the Suzuki–Miyaura coupling of 1-bromo-4-nitrobenzene **3** with PhBpin (pinacol ester of phenylboronic acid, Figure 8). Generally, the three catalysts show deactivation upon reuse, which is expected since the silica suffers from low stability under the strongly basic conditions of the Suzuki–Miyaura and Sonogashira cross-coupling reactions. Here, SBA-15-SH-Pd shows the strongest deactivation. In this field, it has been reported that end-capping of exposed silanols prevents the material from structural damage and extends its activity.[21] Recycling experiments clearly indicate that SBA-15-(1/8-KCl)-Pd is less sensitive than SBA-15-SH-Pd because the wall was occupied by bulky organic groups that increase the hydrophobicity of the material. The most resistant and reusable material in this series was SBA-15-G-Pd, which afforded a yield of 64 % of the coupling product after four runs. As mentioned above, SBA-15-G consists in a condensed material with only SiO$_4$ (Q^4 sites)-walls and low density of silanol groups at the surface. Its robustness and hydrophobicity allow this material to more efficiently resist the harsh alkaline reaction conditions.

Moreover, the enhanced stability of material SBA-15-G compared with material SBA-15-(1/8-KCl) in catalyst recycling experiments may also have its origin in the surface roughness of the materials. Indeed, corrugation of the pore surface of SBA-15-type materials has been evidenced by several research groups.[44] Materials synthesised at low temperature 40 °C < T < 100 °C) display a corrugated pore surface while transversal secondary porous channels were observed with materials synthesised at temperatures ≥130 °C. The parent SBA-15-type silica used for the synthesis of the SBA-15-G-Pd catalyst was synthesised at elevated temperature and therefore features transversal mesoporosity. In contrast, the lower temperature (70 °C) applied in the synthesis of material SBA-15-(1/8-KCl) may lead to materials displaying a higher microporous contribution as a result of higher corrugated pore surface.

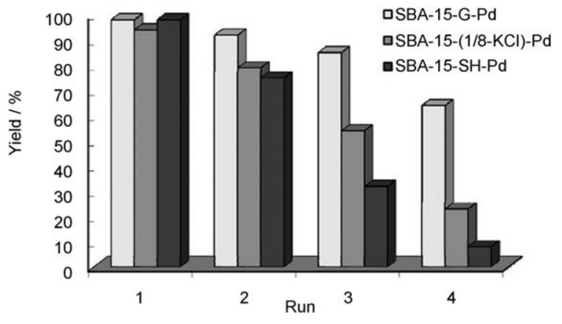

Figure 8. Recyclability of the materials SBA-15-(1/8-KCl)-Pd, SBA-15-G-Pd and SBA-15-SH-Pd in Suzuki–Miyaura coupling reaction of 1-bromo-4-nitrobenzene with PhBpin.

Conclusion

We have reported the synthesis of novel mesoporous silica-based materials featuring SBA-15 architectures and surfaces functionalised with amide–thiol groups. The spectroscopic properties of the materials clearly reflect the synthetic strategies employed for the synthesis of the materials either by post-synthetic grafting or co-condensation reactions. We particularly focussed on the formation of nanostructured materials through “one-pot” hydrolysis–polycondensation reactions. Materials with high structural regularity were obtained from hydrolysis–polycondensation reactions of reaction mixtures containing both at least six equivalents of TEOS and potassium chloride, indicating that the formation of structured materials is governed by siloxy–surfactant interactions.

The catalytic properties of the materials prepared in this study also reflect the synthetic pathways employed and the composition of the materials on a molecular scale. Compared with conventional thiol-functionalised materials obtained from mercaptopropyl-trialkoxysilane precursors, the new thiol-functionalised silica materials reported herein show significantly improved recyclability. This result can be attributed to the higher hydrophobicity of the new materials, induced by the use of the bulkier bis-silylated amide–thiol precursor. In this series, the grafted material SBA-15-G-Pd shows the highest performance in terms of catalytic activity and recyclability. The high stability of this material can be attributed to the high degree of condensation of the silica centres in the mesoporous framework. These results clearly highlight the importance of this feature in the stability and recyclability of silica-based catalysts. Thus parameters such as silanol concentration, degree of condensation, hydrophilicity/-phobicity of the immobilised organic substructure and surface roughness, which are rarely taken into consideration, can have a significant impact on the catalytic properties of heterogeneous silica-based catalysts. For this reason, our results will permit the engineering of more efficient catalysts. For example, recent studies in the Crudden laboratory demonstrated that incorporation of aluminium species in the silica walls of mesoporous materials resulted in a more robust and reusable material.[21] This strategy, in combination with the use of more highly condensed catalysts such as those reported herein, can be applied to the preparation of new catalysts with even higher catalyst lifetimes and recyclability.

Experimental Section

General details: Bis(triethoxysilylpropyl)amine was purchased at ABCR. γ-Thiobutyrolactone and the surfactant Pluronic P123 ($EO_{20}PO_{70}EO_{20}$) were purchased from Aldrich. ^1H and ^{13}C spectra in solution were recorded on Bruker AC 250 or Bruker Avance 400 spectrometers at room temperature. Deuterated chloroform was used as solvent for liquid NMR experiments and chemical shifts are reported as δ values in parts per million relative to tetramethylsilane. IR samples were prepared as KBr pellets. FT-IR spectra were measured on a Perkin–Elmer 1000 FT-IR spectrometer. MS-ESI were measured on a Water Q-Tof mass spectrometer. Solid state ^{13}C and ^{29}Si CP MAS NMR experiments were recorded on a Varian VNMRS 400 MHz solid spectrometer using a two channel probe with 7.5 mm ZrO_2 rotors. The ^{29}Si Solid NMR spectra were recorded using both CP MAS and One Pulse (OP-) sequences with samples spinning at 6 kHz. CP MAS was used to get high signal to noise ratio with 5 ms contact time and 5 s recycling delay. For OP experiments, $\pi/6$ pulse and 60 s recycling delay were used to obtain quantitative information on the silane–silanol condensation degree. The ^{13}C CP MAS spectra were obtained using 5 ms contact time, 5 s recycling delay and 5 kHz spinning rate. The number of scans was in the range 1000–3000 for ^{29}Si OP-MAS spectra and of 2000–4000 of ^{13}C-CP-MAS spectra. Nitrogen sorption isotherms at 77 K were obtained with a Micromeritics ASAP 2020 apparatus. Prior to measurement, the samples were degassed for 10 h at 120 °C. The surface areas (S_{BET}) were determined from BET treatment in the range 0.04–0.3 p/p_0 and assuming a surface coverage of nitrogen molecule estimated to 13.5 Å^2.[45] Pore-size distributions were calculated from the desorption branch of the isotherms using the BdB method.[46] The pore width was estimated at the maximum of the pore-size distribution. TEM images were obtained using JEOL 1200 EX II (120 kV). XRD experiments were carried out with a Bruker D8 Advance AXS (powder diffraction geometry Bragg–Brentano) diffractometer using $Cu_{K\alpha}$ radiation. TGA experiments were performed with a Netzsch TG 209C apparatus. The samples were heated under an air stream from 50 to 800 °C with a heating rate of 10 °C min^{-1}.

Precursor synthesis:

4-Mercapto-N,N-bis(3-(triethoxysilyl)propyl)butanamide ***1***: Under argon, a solution containing (2.55 g, 6 mmol) bis(triethoxysilylpropyl)amine (2.55 g, 6 mmol), γ-thiobutyrolactone (3.10 g, 30 mmol) and toluene (1.5 mL) was heated under reflux during 48 h. After evaporation of the solvent and the excess of γ-thiobutyrolactone under reduced pressure, the title compound was obtained as a viscous liquid. Yield: 3.04 g (5.78 mmol, 96 %). ^1H NMR (400 MHz, $CDCl_3$) $\delta = 0.51$ (m, 4H), 1.15 (m, 18H), 1.26 (t, 1H), 1.57 (m, 4H), 1.88 (q, 2H), 2.38 (t, 2H), 2.53 (q, 2H), 3.19 (m, 4H), 3.75 ppm (m, 12H); ^{13}C NMR ($CDCl_3$) $\delta = 7.4$, 7.5, 18.1, 20.9, 22.4, 24.1, 29.3, 30.9, 48.2, 50.1, 58.1, 58.3, 171.3 ppm; FTIR-(KBr) $\tilde{\nu}_{max} = 2973$, 2930, 2886, 1646, 1107, 610 cm^{-1}; HRMS (ESI+): m/z: calcd for $C_{10}H_{25}NO_7SSi_2$ of the completely hydrolyzed compound: 360.0969 $[M+H]^+$; found 360.0961.

Material syntheses: The materials were synthesised following standard procedures for the preparation of nanostructured mesoporous silica materials of the SBA-15-type.[33] Hydrolysis–polycondensation procedures were performed at 70 °C in the presence of Pluronic P123 (Aldrich) as structure-directing agent using the quantities indicated in Table 1.

Catalysis: In Suzuki–Miyaura coupling reactions, the Pd catalyst (1 mol % Pd; S/Pd = 2:1), the bromoarene (0.25 mmol), K_2CO_3 (70 mg, 0.50 mmol), PhBpin (pinacol ester of phenyl boronic acid, 75 mg, 0.375 mmol) and 1,4-dimethoxybenzene were weighed into a sealed tube with a stirrer bar and flushed with Ar. Dry DMF (2.5 mL, degassed by bubbling Ar) and distilled water (0.125 mL) were added using a syringe. The solution was heated at 80 °C with stirring while monitoring the reaction progress by GC-FID.

In the Sonogashira reaction, the same protocol was adopted. Phenylacetylene (1.5 equiv with respect to the starting aryl halide) was used as alkyne. Na_2CO_3 was used instead of K_2CO_3 in two molar ratios. The reaction temperature was 100 °C.

Acknowledgements

S.E.H. and P.H. thank the program AVERROES (Erasmus Mundus Programme of the European Community) for a doctoral scholarship (S.E.H) and post-doctoral fellowship (P.H). Financial support of the "Reseau de Recherche 3, CPDD" of the CNRS is gratefully acknowledged. A.E.K. and C.M.C. thank the Natural Science and Engineering Council of Canada (NSERC) and Johnson and Johnson for support of this work.

---

[1] a) T. Yanagisawa, T. Shimizu, K. Kuroda, C. Kato, *Bull. Chem. Soc. Jpn.* **1990**, *63*, 988–992; b) C. T. Kresge, M. E. Leonowicz, W. J. Roth, J. C. Vartuli, J. S. Beck, *Nature* **1992**, *359*, 710–712.

[2] a) F. Hoffmann, M. Cornelius, J. Morell, M. Froba, *Angew. Chem.* **2006**, *118*, 3290–3328; *Angew. Chem. Int. Ed.* **2006**, *45*, 3216–3251; b) Y. Wan, D. Y. Zhao, *Chem. Rev.* **2007**, *107*, 2821–2860.

[3] a) A. Corma, *Chem. Rev.* **1997**, *97*, 2373–2419; b) D. Brunel, *Microporous Mesoporous Mater.* **1999**, *27*, 329–344; c) D. Brunel, N. Bellocq, P. Sutra, A. Cauvel, M. Lasperas, P. Moreau, F. Di Renzo, A. Galarneau, F. Fajula, *Coord. Chem. Rev.* **1998**, *178*, 1085–1108.

[4] a) K. Moller, T. Bein, *Chem. Mater.* **1998**, *10*, 2950–2963; b) A. Walcarius, L. Mercier, *J. Mater. Chem.* **2010**, *20*, 4478–4511.

[5] a) L. Nicole, C. Boissiere, D. Grosso, P. Hesemann, J. Moreau, C. M. Sanchez, *Chem. Commun.* **2004**, 2312–2313; b) P. Banet, L. Legagneux, P. Hesemann, J. J. E. Moreau, L. Nicole, A. Quach, C. Sanchez, T. H. Tran-Thi, *Sens. Actuators, B* **2008**, *130*, 1–8; c) A. Quach, V. Escax, L. Nicole, P. Goldner, O. Guillot-Noel, P. Aschehoug, P. Hesemann, J. Moreau, D. Gourier, C. Sanchez, *J. Mater. Chem.* **2007**, *17*, 2552–2560.

[6] a) X. Feng, G. E. Fryxell, L. Q. Wang, A. Y. Kim, J. Liu, K. M. Kemner, *Science* **1997**, *276*, 923–926; b) L. Mercier, T. J. Pinnavaia, *Adv. Mater.* **1997**, *9*, 500–503; c) A. Walcarius, M. Etienne, B. Lebeau, *Chem. Mater.* **2003**, *15*, 2161–2173.

[7] A. M. Liu, K. Hidajat, S. Kawi, D. Y. Zhao, *Chem. Commun.* **2000**, 1145–1146.

[8] a) I. Díaz, J. Perez-Pariente, *Chem. Mater.* **2002**, *14*, 4641–4646; b) L. Beaudet, K. Z. Hossain, L. Mercier, *Chem. Mater.* **2003**, *15*, 327–334; c) A. Walcarius, C. Delacote, *Chem. Mater.* **2003**, *15*, 4181–4192.

[9] J. Brown, L. Mercier, T. J. Pinnavaia, *Chem. Commun.* **1999**, 69–70.

[10] S. N. Che, A. E. Garcia-Bennett, X. Y. Liu, R. P. Hodgkins, P. A. Wright, D. Y. Zhao, O. Terasaki, T. Tatsumi, *Angew. Chem.* **2003**, *115*, 4060–4064; *Angew. Chem. Int. Ed.* **2003**, *42*, 3930–3934.
[11] J. A. Melero, G. D. Stucky, R. van Grieken, G. Morales, *J. Mater. Chem.* **2002**, *12*, 1664–1670.
[12] a) L. Mercier, T. J. Pinnavaia, *Environ. Sci. Technol.* **1998**, *32*, 2749–2754; b) H. M. Kao, T. Y. Shen, J. D. Wu, L. P. Lee, *Microporous Mesoporous Mater.* **2008**, *110*, 461–471; c) T. Kang, Y. Park, J. Yi, *Ind. Eng. Chem. Res.* **2004**, *43*, 1478–1484.
[13] C. Delacôte, F. O. M. Gaslain, B. Lebeau, A. Walcarius, *Talanta* **2009**, *79*, 877–886.
[14] J. D. Webb, S. MacQuarrie, K. McEleney, C. M. Crudden, *J. Catal.* **2007**, *252*, 97–109.
[15] H. Y. Wu, C. T. Chen, I. M. Hung, C. H. Liao, S. Vetrivel, H. M. Kao, *J. Phys. Chem. C* **2010**, *114*, 7021–7029.
[16] W. H. Zhang, X. N. Zhang, L. X. Zhang, F. Schroeder, P. Harish, S. Hermes, J. L. Shi, R. A. Fischer, *J. Mater. Chem.* **2007**, *17*, 4320–4326.
[17] S. V. Mattigod, K. Parker, G. E. Fryxell, *Inorg. Chem. Commun.* **2006**, *9*, 96–98.
[18] a) J. A. Melero, R. van Grieken, G. Morales, *Chem. Rev.* **2006**, *106*, 3790–3812; b) R. D. Badley, W. T. Ford, *J. Org. Chem.* **1989**, *54*, 5437–5443; c) M. H. Lim, C. F. Blanford, A. Stein, *Chem. Mater.* **1998**, *10*, 467–470; d) W. D. Bossaert, D. E. De Vos, W. M. Van Rhijn, J. Bullen, P. J. Grobet, P. A. Jacobs, *J. Catal.* **1999**, *182*, 156–164; e) I. Díaz, C. Marquez-Alvarez, F. Mohino, J. Perez-Pariente, E. Sastre, *J. Catal.* **2000**, *193*, 283–294; f) I. Díaz, C. Marquez-Alvarez, F. Mohino, J. Perez-Pariente, E. Sastre, *J. Catal.* **2000**, *193*, 295–302; g) D. Brunel, A. C. Blanc, A. Galarneau, F. Fajula, *Catal. Today* **2002**, *73*, 139–152; h) K. Wilson, A. F. Lee, D. J. Macquarrie, J. H. Clark, *Appl. Catal. A* **2002**, *228*, 127–133; i) J. Perez-Pariente, I. Diaz, F. Mohino, E. Sastre, *Appl. Catal. A* **2003**, *254*, 173–188; j) I. K. Mbaraka, D. R. Radu, V. S. Y. Lin, B. H. Shanks, *J. Catal.* **2003**, *219*, 329–336; k) Q. H. Yang, J. Liu, J. Yang, M. P. Kapoor, S. Inagaki, C. Li, *J. Catal.* **2004**, *228*, 265–272; l) V. Dufaud, M. E. Davis, *J. Am. Chem. Soc.* **2003**, *125*, 9403–9413; m) K. Shimizu, E. Hayashi, T. Hatamachi, T. Kodama, Y. Kitayama, *Tetrahedron Lett.* **2004**, *45*, 5135–5138; n) Q. H. Yang, M. P. Kapoor, S. Inagaki, N. Shirokura, J. N. Kondo, K. Domen, *J. Mol. Catal. A: Chem.* **2005**, *230*, 85–89; o) B. Rac, P. Hegyes, P. Forgo, A. Molnar, *Appl. Catal. A* **2006**, *299*, 193–201; p) M. Rat, M. H. Zahedi-Niaki, S. Kaliaguine, T. O. Do, *Microporous Mesoporous Mater.* **2008**, *112*, 26–31; q) R. Mouawia, A. Mehdi, C. Reye, R. J. P. Corriu, *J. Mater. Chem.* **2008**, *18*, 4193–4203; r) Y. Tang, S. J. Miao, B. H. Shanks, X. M. Zheng, *Appl. Catal. A* **2010**, *375*, 310–317.
[19] a) C. M. Crudden, M. Sateesh, R. Lewis, *J. Am. Chem. Soc.* **2005**, *127*, 10045–10050; b) Y. Y. Ji, S. Jain, R. J. Davis, *J. Phys. Chem. B* **2005**, *109*, 17232–17238; c) C. M. Crudden, K. McEleney, S. L. MacQuarrie, A. Blanc, M. Sateesh, J. D. Webb, *Pure Appl. Chem.* **2007**, *79*, 247–260.
[20] K. Shimizu, S. Koizumi, T. Hatamachi, H. Yoshida, S. Komai, T. Kodama, Y. Kitayama, *J. Catal.* **2004**, *228*, 141–151.
[21] B. W. Glasspoole, J. D. Webb, C. M. Crudden, *J. Catal.* **2009**, *265*, 148–154.
[22] S. MacQuarrie, B. Nohair, J. H. Horton, S. Kaliaguine, C. M. Crudden, *J. Phys. Chem. C* **2010**, *114*, 57–64.
[23] a) F. Y. Zhao, M. Shirai, Y. Ikushima, M. Arai, *J. Mol. Catal. A: Chem.* **2002**, *180*, 211–219; b) S. S. Pröckl, W. Kleist, M. A. Gruber, K. Kohler, *Angew. Chem.* **2004**, *116*, 1917–1918; *Angew. Chem. Int. Ed.* **2004**, *43*, 1881–1882; c) N. T. S. Phan, M. Van Der Sluys, C. W. Jones, *Adv. Synth. Catal.* **2006**, *348*, 609–679; d) S. MacQuarrie, J. H. Horton, J. Barnes, K. McEleney, H. P. Loock, C. M. Crudden, *Angew. Chem.* **2008**, *120*, 3324–3328; *Angew. Chem. Int. Ed.* **2008**, *47*, 3279–3282; e) J. M. Richardson, C. W. Jones, *J. Catal.* **2007**, *251*, 80–93.
[24] C. E. Garrett, K. Prasad, *Adv. Synth. Catal.* **2004**, *346*, 889–900.
[25] K. Königsberger, G. P. Chen, R. R. Wu, M. J. Girgis, K. Prasad, O. Repic, T. J. Blacklock, *Org. Process Res. Dev.* **2003**, *7*, 733–742.
[26] W. Schmidt, *ChemCatChem* **2009**, *1*, 53–67.
[27] a) P. Rollet, W. Kleist, V. Dufaud, L. Djakovitch, *J. Mol. Catal. A: Chem.* **2005**, *241*, 39–51; b) C. W. Jones, M. Tsapatsis, T. Okubo, M. E. Davis, *Microporous Mesoporous Mater.* **2001**, *42*, 21–35.
[28] P. Van der Voort, C. Vercaemst, D. Schaubroeck, F. Verpoort, *Phys. Chem. Chem. Phys.* **2008**, *10*, 347–360.
[29] a) B. Gadenne, P. Hesemann, J. J. E. Moreau, *Chem. Commun.* **2004**, 1768–1769; b) B. Gadenne, P. Hesemann, V. Polshettiwar, J. J. E. Moreau, *Eur. J. Inorg. Chem.* **2006**, 3697–3702; c) T. P. Nguyen, P. Hesemann, M. L. T. Thi, J. J. E. Moreau, *J. Mater. Chem.* **2010**, *20*, 3910–3917.
[30] T. P. Nguyen, P. Hesemann, P. Gaveau, J. J. E. Moreau, *J Mater. Chem.* **2009**, *19*, 4164–4171.
[31] B. Nohair, S. MacQuarrie, C. M. Crudden, S. Kaliaguine, *J. Phys. Chem. C* **2008**, *112*, 6065–6072.
[32] A. Derrien, PhD Thesis, Université de Montpellier II (France), **2001**.
[33] A. El Kadib, P. Hesemann, K. Molvinger, J. Brandner, C. Biolley, P. Gaveau, J. J. E. Moreau, D. Brunel, *J. Am. Chem. Soc.* **2009**, *131*, 2882–2892.
[34] D. Massiot, F. Fayon, M. Capron, I. King, S. Le Calve, B. Alonso, J. O. Durand, B. Bujoli, Z. H. Gan, G. Hoatson, *Magn. Reson. Chem.* **2002**, *40*, 70–76.
[35] W. P. Guo, J. Y. Park, M. O. Oh, H. W. Jeong, W. J. Cho, I. Kim, C. S. Ha, *Chem. Mater.* **2003**, *15*, 2295–2298.
[36] J. Yu, J. L. Shi, H. R. Chen, J. N. Yan, D. S. Yan, *Microporous Mesoporous Mater.* **2001**, *46*, 153–162.
[37] K. Mortensen, J. S. Pedersen, *Macromolecules* **1993**, *26*, 805–812.
[38] B. L. Newalkar, S. Komarneni, *Chem. Commun.* **2002**, 1774–1775; B. L. Newalkar, S. Komarneni, *Chem. Mater.* **2001**, *13*, 4573–4579.
[39] a) R. Chinchilla, C. Najera, *Chem. Rev.* **2007**, *107*, 874–922; b) E. Negishi, L. Anastasia, *Chem. Rev.* **2003**, *103*, 1979–2017.
[40] K. Sonogashira, Y. Tohda, N. Hagihara, *Tetrahedron Lett.* **1975**, *16*, 4467–4470.
[41] a) N. Miyaura, A. Suzuki, *Chem. Rev.* **1995**, *95*, 2457–2483; b) N. Miyaura, T. Yanagi, A. Suzuki, *Synth. Commun.* **1981**, *11*, 513–519.
[42] K. Sonogashira, *J. Organomet. Chem.* **2002**, *653*, 46–49.
[43] N. Hoshiya, N. Isomura, M. Shimoda, H. Yoshikawa, Y. Yamashita, K. Iizuka, S. Tsukamoto, S. Shuto, M. Arisawa, *ChemCatChem* **2009**, *1*, 279–285.
[44] a) M. Kruk, M. Jaroniec, C. H. Ko, R. Ryoo, *Chem. Mater.* **2000**, *12*, 1961–1968; b) A. Galarneau, H. Cambon, F. Di Renzo, F. Fajula, *Langmuir* **2001**, *17*, 8328–8335; c) V. B. Fenelonov, A. Y. Derevyankin, S. D. Kirik, L. A. Solovyov, A. N. Shmakov, J. L. Bonardet, A. Gedeon, V. N. Romannikov, *Microporous Mesoporous Mater.* **2001**, *44*, 33–40; d) A. Zukal, H. Siklova, J. Cejka, *Langmuir* **2008**, *24*, 9837–9842; e) C. J. Gommes, H. Friedrich, M. Wolters, P. E. de Jongh, K. P. de Jong, *Chem. Mater.* **2009**, *21*, 1311–1317.
[45] S. Brunauer, P. H. Emmett, E. Teller, *J. Am. Chem. Soc.* **1938**, *60*, 309–319.
[46] J. C. P. Broekhoff, J. H. de Boer, *J. Catal.* **1968**, *10*, 377–390.

Received: July 30, 2010
Revised: March 3, 2011